A Diagnostic Approach for Electro-Mechanical Actuators in Aerospace Systems

Edward Balaban
NASA Ames Research Center
Moffett Field, CA, 94035
650-604-5655
edward.balaban@nasa.gov

Abhinav Saxena
Research Institute for Advanced Computer Science
NASA Ames Research Center
Moffett Field, CA, 94035

Prasun Bansal
Mission Critical Technologies, Inc.
NASA Ames Research Center
Moffett Field, CA, 94035

Kai F. Goebel
NASA Ames Research Center
Moffett Field, CA, 94035

Paul Stoelting
Moog Inc.
East Aurora, NY 14052

Simon Curran
Moog Inc.
East Aurora, NY 14052

Abstract—Electro-mechanical actuators (EMA) are finding increasing use in aerospace applications, especially with the trend towards all all-electric aircraft and spacecraft designs. However, electro-mechanical actuators still lack the knowledge base accumulated for other fielded actuator types, particularly with regard to fault detection and characterization. This paper presents a thorough analysis of some of the critical failure modes documented for EMAs and describes experiments conducted on detecting and isolating a subset of them. The list of failures has been prepared through an extensive Failure Modes and Criticality Analysis (FMECA) reference, literature review, and accessible industry experience. Methods for data acquisition and validation of algorithms on EMA test stands are described. A variety of condition indicators were developed that enabled detection, identification, and isolation among the various fault modes. A diagnostic algorithm based on an artificial neural network is shown to operate successfully using these condition indicators and furthermore, robustness of these diagnostic routines to sensor faults is demonstrated by showing their ability to distinguish between them and component failures. The paper concludes with a roadmap leading from this effort towards developing successful prognostic algorithms for electromechanical actuators. [1] [2]

TABLE OF CONTENTS

[1] 978-1-4244-2622-5/09/$25.00 ©2009 IEEE.
[2] IEEEAC paper #1345, Version 4, Updated January 9, 2009

1. INTRODUCTION

Electro-mechanical Actuators are used in a variety of aerospace applications, from civilian airliners to robotic spacecraft. Although EMAs are still relative newcomers to the aerospace field the concept of all-electric aircraft and spacecraft designs promises an even wider use of EMAs in the future at the expense of hydraulic actuators. Actuators are safety-critical components of an aerospace system and an undetected actuator failure can lead to serious consequences. Even though actuators have been studied extensively from a functional point of view - in order to help develop new and improved designs - feedback from the field is still needed for a better understanding of various fault modes of the often complex EMA assemblies. EMA fault diagnosis poses an interesting research problem as it is composed of electrical, electronic, and mechanical subsystems, which results in intricate failure modes and effects. Any fault in these sub-assemblies needs to be successfully and efficiently detected, identified, and isolated using a limited set of sensor signals available. Aerospace applications in particular have very strict constraints on weight and volume, where multiple redundant systems come with considerable cost and weight penalty. In order to fulfill the stringent reliability requirements, an actuator with no hardware redundancy must be equipped with a sophisticated diagnostic, prognostic, and recovery system. Since the current generation of actuators is often under-instrumented, physics-based modeling of failure modes and mechanisms can help make the most of the available measurements. Furthermore, given the strict safety considerations of aerospace systems, a health management system must leave enough time for contingency management before a catastrophic event may take place. Early fault detection lays the foundation of successful prognostic and mitigation steps. The desire to obtain early fault detection, however, must be balanced against the need to keep false positive rates low. False negatives not only reduce the diagnostic confidence, but can also result in unnecessary, yet often costly and

disruptive, mitigation actions. Therefore, the quality of the health management system can have a direct impact on the performance of the client actuator.

Of the various kinds of actuators, EMAs were chosen for this study because of their growing role in the aerospace field. They are relatively compact and can offer high power-to-weight ratios and motion velocities. We also decided to concentrate on actuators suitable for use with flight control surfaces, to build on the previous F-18 flight experiments at NASA Dryden Flight Research Center [1], which led us to the choice of linear, ballscrew type EMAs.

In the next section we present a discussion on various EMA fault modes, including the most common sensor faults. A summary of fault modes has been presented based on our literature search and interactions with the industry. We then describe the experimental setup and the data acquisition, system, followed by a detailed discussion of the new diagnostic system. Results are presented next, followed by a discussion and plans for future work.

2. EMA FAULTS

Since EMAs, as mentioned earlier, are relatively new to the field of aerospace, they have not yet been deployed for a long enough time or in large enough numbers to accumulate reliable fault statistics. Most of the commercial airliners in service still rely on hydraulic actuation for their primary flight surfaces, landing gear, and other major components. Small EMAs are sometimes used for secondary functions, such as trim tabs actuation and spoiler or speed break deployment. The situation is similar in military applications, where most of the aircraft in the active inventory rely on hydraulic actuation, although there are efforts currently under way to deploy electro-mechanical actuators in utility roles (landing gear, aerial refueling doors, and weapons bay doors) in the future models of some of the new designs, such as the F-35 Joint Strike Fighter.

Recently designed commercial aircraft, such as Boeing 787 or Airbus 380, are also starting to use more EMAs in the roles traditionally reserved for hydraulic systems. On the 787, for example, EMAs, in addition to spoilers and trim actuation, operate landing gear breaks and are part of the environmental control system.

Space vehicles currently use EMAs for functions such as positioning of antennas and movement of robotic arms, with some of the future rocket launcher designs intending to use EMAs for their thrust vector control. The challenges with obtaining performance statistics in this domain are that only a small number of each vehicle type are usually built and that the onboard actuators are rarely used for more than a few hours total throughout the entire service life of a vehicle.

The fault and failure information for EMAs (summarized in tables 1, 2, 3, and 4) came primarily from the following sources: Failure Modes, Effects, and Criticality Analysis (FMECA) information provided by Moog Corporation; published industrial information [2, 3]; information from the US military reports [4]; as well as from our general survey of publications related to actuator diagnostics [5, 6].

The faults in the tables 1, 2, 3, and 4 are loosely distributed among four general categories: sensor, mechanical or structural, motor, and power or electrical. Some of the faults, such as return channel jam, are specific to linear, direct-drive ballscrew electromechanical actuators which are the primary focus of our research. Others, such as motor or electrical faults, are applicable to a wider range of EMAs.

Each of the fault modes is presented along with the failure mode it can lead to, if not diagnosed and remedied in time. The transition from fault to failure in EMAs and prediction of their remaining useful life is the subject of our ongoing research. The probability and criticality numbers refer to the fault modes and are presented in an abstracted form, on a scale from 1 to 10. This was done both to protect proprietary information and to aggregate data collected from the various sources in a unified manner.

We also included suggestions on the general approach for diagnosing and prognosing each fault type – model based, data-driven, or hybrid. This was mainly done for our own research planning purposes, although we hope that it may be of some value to the reader as well. The prototype diagnostic system developed for this particular effort utilized data-driven methods only; we do, however, have physical models of varying degrees of fidelity currently under development as well.

Mechanical/Structural Faults

Mechanical and structural faults are likely to be the main source of concern for electro-mechanical actuators deployed in the demanding conditions of aerospace applications. Their main causes are excessive loads, environmental factors, lubrication issues, and manufacturing defects. This class of faults has been the primary focus of our research for some time, as we feel that out of all the actuator components, these have the fewest number of effective diagnostic and prognostic methods developed for at present.

One of the exceptions to the above observation, however, is bearing faults. They have been subjects of extensive studies over the course of the last few decades and, therefore, were not pursued as part of ours. Interested reader can refer to [7, 8], for instance, as a starting point on the subject. Faults germane to multi-channel EMAs (which utilize multiple motors via a transmission) or to geared actuators are not covered in this paper either. They may be a subject of our future work.

Motor Faults

Motor faults are the next most important category of EMA faults. Motors are often operated at high rotational rates,

leading to increased temperatures within their housing and significant mechanical stresses - thus making them prone to developing winding shorts, rotor shaft eccentricities, and other problems.

There have been several thorough research efforts in the recent years on the subject of electrical motor faults [5, 6, 9]. There is still, however, a need for further research, therefore this class of faults remain high on our interest list and will be incorporated in into our upcoming experiments.

Electrical/Electronic Faults

The characteristics of electrical and electronic faults in the power and control systems of EMAs do not differ significantly from the same type of faults in other aerospace systems. The Diagnostics & Prognostics Group at NASA Ames has a team dedicated to conducting research in this domain. Some of their accomplishments are described in [10, 11]. In this paper we list only the most likely or significant faults of this category, without going into too much detail.

Sensor Faults

A study to classify and diagnose sensor faults common to aerospace applications was conducted in parallel with the development of the EMA diagnostic system and represented a significant research effort in its own right. It will be the subject of a separate paper; we will, however, describe modeling and diagnosis of sensor faults seeded along with the actuator system faults for this series of experiments.

Table 1 below summarizes the general categories of sensor faults used in our work and provides estimates of the range and median values of their parameters, as identified during our literature review [12-16]

Table 1 –Sensor Fault Categories.

Fault	Range	Median	Remarks
Bias	1.2% to 60%	20%	% change over the nominal value
Scaling	0.3 to 0.7	0.45	Scale Factor
	2.5 to 4.8	3.28	Scale Factor
Drift	6% to 75%	29%	% change over the nominal value, reported at the end of the drift (or data set)
Noise	2.5% -to 250%	20%	% peak to peak values over the nominal value
Intermittent Dropout	2 to 10 drops	8 drops	Over a range of 20% to 29% of the reported data set, with median range of 23%

Experiments described in this paper covered bias, scaling, and drift faults only. Noisy sensors and intermittent dropouts will be incorporated in the near future. Due to the current equipment limitations, as described in the later sections, the sensor faults were simulated in software.

Subset of Fault Modes Selected for the Study

Along with the sensor faults described in the previous section, two mechanical faults were selected as the injected faults in our experiments:

Return channel jam: return channel is a component of a ballscrew actuator that transports balls in the circuits within the nut from the end of a circuit back to its beginning, as the nut travels along the rotating screw. A jam in the return channel, caused, for example, by a piece of debris or a deformed ball, would stop that circulation and cause the ballscrew to behave similarly to a much less efficient jackscrew (also known as the acme screw). Modern ballscrew actuators usually incorporate multiple independent ball motion circuits, thus a jam in one of them would not be catastrophic, but would still lead to a greatly decreased efficiency and remaining useful life of an actuator. A highly rare situation of all of the channels getting jammed would likely lead to severe damage of the nut within a short period of time.

Return channel jam is of particular interest to us because it is a fault that cannot easily be addressed by design modifications.

Spalling: spalling refers to the development of indentations in metal surfaces at high stress contact points. A severe case of a spall may result in metal flakes separating from the surface, creating potentially dangerous debris. In the case of a ballscrew, where the contact surfaces of the nut and the screw (as well as the balls) may be subject to spalling, one of the consequences may be increased vibration, which can lead to damage of other actuator components. The likelihood of an EMA developing a spall in one of its components over its lifetime is not insignificant.

Table 2 – Mechanical/Structural Fault Modes.

Component	Fault	Failure	Relative Probability (1-10, low to high)	Relative Criticality (1-10, low to high)	Suggested Model Type (Physics, Data/Trending, Hybrid)
screw	spalling (mild)	severe vibrations, metal flakes separating	5	3	Hybrid
	excessive wear/backlash	severe backlash	7	3	Data/Trending
nut	spalling (mild)	severe vibrations, metal flakes separating	5	3	Hybrid
	backlash	severe backlash	7	3	Data/Trending
	degraded operation	seizure/disintegration	3	5	Data/Trending
	binding/sticking	seizure/disintegration	3	3	Data/Trending
	bent/dented/warped	seizure/disintegration	1	5	Data/Trending
ball return(s)	jam	seizure/disintegration	5	8	Hybrid
bearings	spalling	severe vibrations, metal flakes separating	5	3	Hybrid
	binding/sticking	seizure/disintegration	2	4	Data/Trending
	corroded	severe vibrations, metal flakes separating, seizure/disintegration	2	5	Hybrid
	backlash	severe backlash, vibration, disintegration	7	3	Data/Trending
piston	crack(s), slop/play	structural failure	1	10	Data/Trending
dynamic seals	wear	structural failure	4	6	Physics
	structural failure	same	3	8	Data/Trending
static seals	structural failure	same	2	8	Data/Trending
balls	Spalling/deformation	severe vibrations, metal flakes separating	5	3	Hybrid
	excessive wear	backlash	7	5	Hybrid
mountings	crack(s), slop/play	complete failure	1	7	Data/Trending
lubricant	contamination	seizure/disintegration	8	5	Data/Trending
	chemical breakdown	seizure/disintegration	4	5	Physics
	run-dry	seizure/disintegration	3	10	Hybrid

Table 3 –Motor Fault Modes.

Component	Fault	Failure	Relative Probability (1-10, low to high)	Relative Criticality (1-10, low to high))	Suggested Model Type (Physics, Data/Trending, Hybrid)
connectors (for stator coils, resolver, RTD, brake coil, and ground)	degraded operation (can manifest itself as increased resistance)	disconnect	5	6	Data/Trending
	intermittent contact	disconnect	3	7	Data/Trending
stator	stator coil fails open (results in degraded EMA performance)	same	4	4	Physics
	insulation deterioration / wire chafing (manifests itself via reduced or intermittent current through stator coil or intermittent shorts)	short circuit	5	5	Data/Trending
resolver	coil fails open (this and the other resolver faults can result in inaccurate position reports, EMA performance deterioration)	same	4	10	Physics
	intermittent coil failures	permanent coil failure	5	7	Data/Trending
	insulation deterioration / wire chafing	short circuit	5	7	Data/Trending
rotor and magnets	rotor-magnets chemical bond deterioration	complete magnet separation, likely leading to motor failure	2	10	Data/Trending
	rotor eccentricity	support bearing failure	3	6	Physics

Table 4 – Electrical/Electronic Faults.

Component	Fault	Failure	Relative Probability (1-10, low to high)	Relative Criticality (1-10, low to high)	Suggested Model Type (Physics, Data/Trending, Hybrid)
Power supply	short circuit	same	5	10	Hybrid
	open circuit	same	5	10	Hybrid
	intermittent performance	short circuit or open circuit	5	8	Data/Trending
	thermal runaway	dielectric breakdown of components, leading to open or short circuits	6	10	Hybrid
Controller capacitors	dielectric breakdown	short circuit or open circuit	4	8	Hybrid
Controller transistors	dielectric breakdown	short circuit or open circuit	4	8	Hybrid
Wiring	short circuit	same	5	10	Hybrid
	open circuit	same	5	10	Hybrid
	insulation deterioration / wire chafing	short circuit or open circuit	5	8	Data/Trending
Solder joints	intermittent contact	disconnect	5	8	Hybrid

3. DATA ACQUISITION

Figure 1 – Moog MaxForce 883-023 test actuator.

A ballscrew electromechanical actuator was used as the test article in our experiments. The experiments were performed on a stand located at Moog Inc. The test actuator, Moog MaxForce 883-023 (Figure 1), was connected to the hydraulic load cylinder by a rotating horn as shown in Figure 2Figure 2.

Control and data acquisition were performed by real-time software running on dSPACE platform. Table 5 contains a list of all of the sensors used on the test platform, as well as their associated sampling frequencies.

Vibration was measured at four points on the test actuator, as shown in Figure 3. All three axes of vibration were measured, with an additional measurement in the Z-direction by the accelerometer mounted directly on the nut of the ball screw. Temperature measurements were provided by a T-type thermocouple on the nut and an RTD embedded in the stator of the motor, as shown in Figure 3.

Figure 2 – EMA test stand at Moog Corp.

Table 5 - List of Sensors.

Measurement	Sensor	Type	Sample Rate
Load	Model 75 Sensotec Load Cell	Bonded foil strain gage compression and tension	3 kHz
Position	Trans-Tek 0219-0000	LVDT	3 kHz
Nut Temperature	T-type Thermo-couple	Copper-constantan thermocouple	3 kHz
Motor Temperature	Integrated Stator RTD	RTD (thermistor)	3 kHz
Torque Producing Current	T200 Motor Drive Output	Hall effect sensor	3 kHz
Motor Velocity	T200 Motor Drive Output	Resolver	3 kHz
3-Phase Currents	(3) LEM LA 25-P Current Transducers	Closed loop (compensated), works on Hall effect	24 kHz
X-Y-Z Accelerometers	(3) PCB Model 352A24	Piezoelectric ceramic, shear	24 kHz
Nut Accelerometer	PCB Model 352A24	Piezoelectric ceramic, shear	24 kHz

Load is sensed by a Model 75 Sensotek 50,000 lbf. load cell. The position of the rod end of the test actuator was measured by a Trans-Tek 0219-0000 Linear Differential Voltage Transducer (LVDT).

LEM LA 25-P current transducers were used on each motor phase to sense the phase currents. For data acquisition, the Moog T200 motor drive output an analog signal representing the torque producing current, as well as the motor velocity.

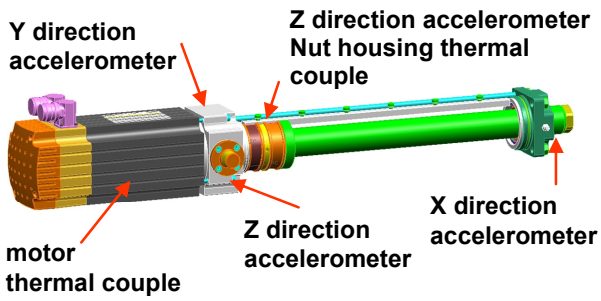

Figure 3 - Location of sensors on Moog MaxForce 883-023 actuator.

Table 6 - Experiments performed with seeded mechanical faults.

Experiment Set	Description
Baseline	Data collected with a nominal actuator just before the first set of ball return jam tests.
One Ball Return Jammed	One of the return channels fully blocked. Simulates obstruction of the return channel by a detached piece of insulation or other debris.
Repeatability	Tests to determine whether disassembly and reassembly of actuators affects test results. Five-back-to back runs were conducted.
Backlash	Tests with undersized balls to simulate backlash (freeplay)
Spalling	The purpose of this series of tests was to determine if a surface flaw (spall) can be detected using the actuator sensor suit. Three flaws have been electro-discharge machined into the screw of the actuator. The flaws were machined into the entire root of the screw forming a continuous flaw from crest to crest.

Tests Performed

Table 6 describes the types of mechanical component fault cases introduced during the tests.

Sensor faults were injected a posteriori, as described in the next section. Permutations of the conditions below were used to develop 8 scenarios for each of the mechanical component fault cases:

- Motion profile: sinusoid or triangular wave

- Load type: constant or spring

- Load level: low (860 lbs spring force, 900 lbs constant force) or high (1725 lbs spring force, 1800 lbs constant force)

For the purposes of training and testing a neural network based classifier, described in the subsequent sections, extended duration scenarios were created using the collected data. These scenarios were designed to preserve the character of the collected data as much as possible, while extending the duration to 180 seconds. They contain two segments each – nominal, to represent a healthy system before the fault occurred and a faulty segment (90 seconds each). Since on the test stand the faults had to be seeded before the start of the tests (due to hardware limitations), nominal data was chosen from the experiments conducted under the same conditions. The total number of scenarios produced was 48: 8 (conditions) x (2 components faults + 4 sensor faults).

Sensor Fault Simulations

Bias: Here bias was specified as percentage of the average baseline temperature (80F), calculated over the set of nominal (no fault injected) scenarios. Bias was injected into temperature sensor data. Gaussian noise was then introduced into the actual amount of bias added, with the signal-to-noise ratio (SNR) of 5 (see Figure 4).

Drift: this fault was also injected into the nut temperature data. The fault was defined by specifying drift velocity (distance traveled in a certain period of time). The length of constant drift velocity segments was randomized (max 1000 data points) and Gaussian noise introduced into velocity value itself – so for each segment the velocity may be somewhat different from its neighbors. The signal-to-noise ratio for the later was set to 5.

Scaling: the signal is amplified by the scaling factor, also with Gaussian noise injected (SNR of 5).

Loss of Signal: sensor data from the point of failure replaced by all zeros.

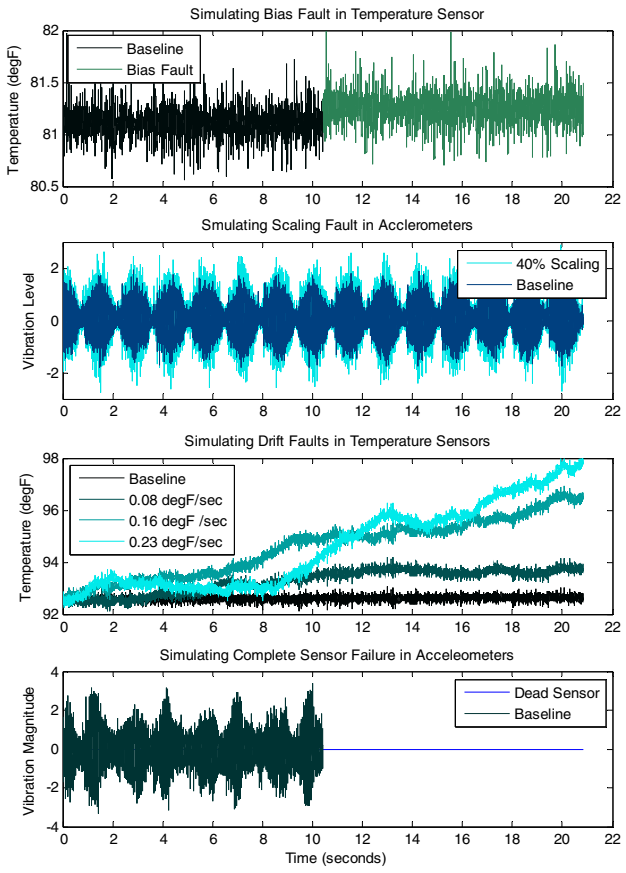

Figure 4 – Sensor fault simulations.

4. Feature Extraction and The Diagnostic System

Given the complexity of the experimental data and the variety of failure modes (actuator and sensor failures), a diagnostic system based on Artificial Neural Networks (ANN) was designed. A comprehensive analysis of data was carried out to extract a set of uncorrelated features that would not only detect various fault modes but also disambiguate between sensor and system faults. Keeping the latter requirement, the confusion matrix (Table 9) was further partitioned into sections that helped to interpret the results. This section explains the implementation details and enumerates the key aspects of the classifier diagnostic system.

Feature Extraction

Appropriate feature extraction lays the foundation of a successful (accurate and reliable) diagnostic system. For a successful practical implementation it is desirable that features not only be computationally inexpensive but also be explainable in physical terms. Furthermore, they should be characterized by a) large between-class and small within-class variance, b) should be fairly insensitive to external variables like noise, and c) should be uncorrelated with other features. Keeping these requirements in mind, we selected a set of seven sensor-feature pairs that were expected to detect and distinguish seven distinct modes of the system: a healthy system, two actuator fault modes, and four different sensor faults (see Table 7). Based on an extensive literature search (see Section 2), sensor faults were generated with parameters representative of the real world. Specifically, a bias of 20% value of peak-to-peak temperature signal magnitude, a temperature sensor drift with drift velocity of 0.02 °F/sec, a scaling factor of 1.5 times the original signal peak-to-peak amplitude, and a zero output (dead sensor) case were simulated using the baseline data to include various sensor faults.

Table 7 - Fault vs. Feature Matrix.

Faults	Features						
	TD_{Nut}	TD_{Motor}	SD_x	SD_y	SD_Z	DI_{Motor}	DI_{Nut}
Return Channel Ball Jam	X	X	X	X	X		
Spall			X	X	X		
Nut thermocouple Drift	X						X
Nut thermocouple Bias	X						
Z Accel. Scaling					X		
X Accel Complete Failure			X				

In addition, since there were several different experimental conditions that considerably affect the sensor measurements, two additional features were designed that characterize these experimental conditions. These features are described below Table 8 gives an overview of all the features and their significance with respect to different system modes they identify. Features were calculated every half a second on a one second long sliding window. Thus for each 90 second long segment (under various conditions) 180 feature points were generated.

Load Profile Indicator (LPI)

Experiments were conducted under two different load profiles, namely sinusoidal and triangular, to cover two extremes of smooth and drastic movements around the point of direction reversal. However, in practice, it is expected that a real load profile would lie somewhere in between these two situations. Since a significant difference was observed in sensor measurements under different load profiles, a feature called Load Profile Indicator (LPI) was developed to numerically represent the roughness of motion. Each one second sampling window is further subdivided into smaller sub-segments of 0.002 seconds and a local slope is calculated for each sub-segment. A variance of absolute values of the slope from these segments is then computed as a feature for operational condition. Triangular profile results in a smaller (near zero) variance, where as a pure sinusoidal profile results in a higher variance due to smooth peaks. Any combination of triangular and sinusoid segments appropriately results in a representative variance as shown in Figure 5.

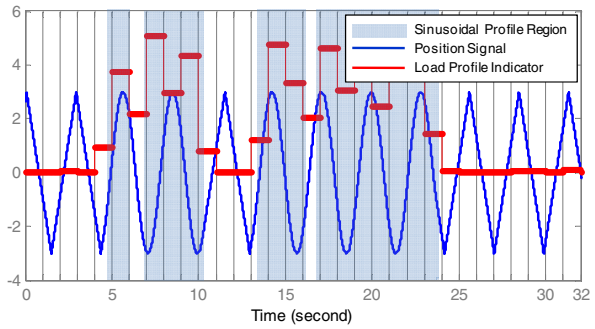

Figure 5 - Load Profile Indicator (LPI).

Force Indicator (FI)

Loads were applied under two types of forces: opposing force and spring force. In the case of opposing force motion, a constant force is experienced by the system, whereas for spring motion the force is proportional to the displacement from the neutral position. Computing FI for opposing force is trivial; however, for spring force motion force indicators were computed by assessing the value of spring-constant (k) at peak position displacements and using them to calculate corresponding forces at all other positions. Thus, in addition to the seven features derived from sensor (Table 7) these two condition features were input as part of a nine point vector to the classifier system (described next).

Diagnostic Classifier

A three layer Artificial Neural Network (ANN) was implemented as a multi-category classifier to distinguish between the seven states of the system health. The first layer consisted of nine nodes, with tansigmoid transfer functions,

one for each feature in the input feature vector. The hidden layer had five nodes with logsigmoid transfer function and the output layer had seven nodes with logsigmoid transfer functions, one for each of the seven classification categories. All input features were continuous, real-valued and were standardized to have zero mean and unit variance [17]. Binary targets were assigned such that of the seven output bits only the correct category bit turned 1 and the rest stayed 0. Initial weights for the network were chosen based on standardized input ranges to ensure uniform learning [17]. Networks were trained using the resilient back-propagation (RPROP) algorithm [18]

Evaluation Procedure & Results

Data were divided into two sets for training and testing purposes, based on the experiment load levels. The network was trained on low load conditions (~900lbs) and was tested for high load (~1800lbs) conditions. In order to obtain a meaningful statistic, 30 ANNs were trained and tested for each experiment and the results averaged. Training was carried out for 200 epochs. Results were further aggregated in the form of a confusion matrix as shown below in Table 9 to observe the False Positive rate (FP), False Negative rate (FN), Misclassification rate (MC), and Non-Identification rate (NI). The rows in the confusion matrix represent true state of the system and the columns represent estimated states. As shown, misclassification rate is observed as a measure of disambiguation between component faults and sensor faults and as non-identification rate for cases that are not identified as any of the predefined classes. Each category is computed as a percentage of the total number of observed instances in the respective classes.

Table 9 - Confusion matrix for two component faults and four sensor faults.

		NF	***CF1***	***CF2***	***SF1***	***SF2***	***SF3***	***SF4***
	NF	TP	FP					
	CF1	FN	TP		MC			
	CF2			TP				
NI	***SF1***		MC		TP			
	SF2					TP		
	SF3						TP	
	SF4							TP

Table 8 –Diagnostic Classifier Features.

Feature	Sensors	Definition	Fault Modes	Rationale
Temperature Deviation (TD)	Nut thermocouple, Motor thermocouple	Absolute deviation from nominal temperature range	Spall, jam, sensor bias	Nut temperature rises due to increased friction from spalled nut. Motor temperature rises due to increased current levels to counter increased resistance Temperatures also change due to bias
Drift Indicator (DI)	Nut thermocouple, Motor thermocouple	A binary feature that assumes the value *one*, if a finite rate of change of temperature is detected within the sampling window, and *zero* otherwise	Sensor drift	Monitoring over some period of time can help identify sensor drift and distinguish it from bias, which is not expected to change continuously in shorter time-intervals
Signal Standard Deviation (SD)	Accelerometers: X, Y, Z on motor housing and one on the Nut	Standard deviation of the signal within one sampling window	Jam, dead sensor	Jam reflects in increased vibrations of the accelerometers mounted on the motor. Dead sensor results in zero output
Load Profile Indicator	Position sensor	Characterizes the smoothness of load profiles ranging between smooth sinusoids to rough triangular profiles	All	Nature of load the profile significantly changes the vibration signature of the system. This difference should be distinguished from failure signatures
Force Indicator	Position sensor	Assesses the force on actuator. For opposing force motion the force remains constant, proportional to peak loads. For spring motion force varies with the position and is a fraction of the peak loads	All	Given combinations of two different load conditions and two load application methods, differences in corresponding sensor signatures should be distinguished from fault signatures

5. RESULTS & DISCUSSION

Based on the procedure described above, a total of 3.46% false positive rate, 1.21% false negative rate, and 0.29% misclassification rates were observed. About 3.8% cases were not identified under any of the defined categories. Upon careful observation, it was realized that the relatively high value for non-identification rate can be attributed to several factors. First, the experiments were conducted under multiple conditions of load levels, load types, and load profiles. Each of these conditions affects the baseline measurements in their own ways, often overlapping with the affects produced by various components and sensor faults. For instance, nut temperature may be observed to increase due to ball jam, thermocouple bias, or thermocouple drift faults. However, high loads result in higher temperatures than low loads and spring motion load profile consistently results in higher temperatures. These changes in load characteristics result in difference in baseline conditions themselves and hence, if not appropriately trained, a classifier finds it difficult to point to any specific reason for such effects. Furthermore, no information regarding ambient temperatures was available from the experimental data. It must be noted that ambient temperatures can affect the baseline measurements as well. Since we partitioned the experimental data into high and low load sets, the classifier did not get a good chance to learn the effects of the load levels and, consequently, the ability to distinguish them from other effects that cause such overlapping variations (it also points to a more fundamental weakness of data-driven approaches). Similar effects are not only limited to temperature variations, but also to the vibration levels measured through accelerometers.

6. PLANS FOR FUTURE WORK

There are a number of different avenues for future work. Longer duration experiments will be conducted to better characterize the effects of external factors and obtain more consistent training and testing data. This will also provide steady state measurements to establish repeatable baselines as well as reveal dynamic effects of the seeded fault conditions. Experiments under controlled conditions will be conducted to characterize the effects of external environment, loading conditions, various fault modes, and severity of those faults. Other experiments will be conducted to develop techniques for detecting motor faults (e.g. rotor shaft eccentricity and winding insulation degradation) and mechanical faults requiring high precision, high resolution position sensing (e.g. backlash). To that end, plans are under way to carry out experiments on a new actuator test stand (Figure 6) at NASA Ames by seeding faults into the test actuator and the sensing system and observing their signatures while the system operates under a variety of load conditions. The new test stand incorporates a powerful electro-mechanical load actuator (Moog 886 series), capable of generating up to five metric tons of force. The flexible design of the stand accommodates test actuators of various sizes and configurations and its control system allows creation of fully customizable load and motion profiles. The sensor suite features a load cell, accelerometers, as well as high-precision position, current, and temperature sensors.

Classifiers rely on features to allow optimal detection and disambiguation between system and sensor faults. While the features described herein are focused mostly on the time domain, other categories of features (e.g., frequency-based) should be considered. As more data becomes available, more sophisticated features will be explored for improving the diagnostic performance. Another direction for future work is the verification of dynamic models being developed for actuator systems. These models will then be employed in hybrid diagnostic and prognostic techniques. Sensor fault models validation and verification is yet another potential direction. Experiments with seeded sensor faults on real systems should be conducted to confirm that the models behave correctly. In practice, sensor fault detection should go hand-in-hand with accommodation strategies. The understanding of underlying mechanisms of sensor faults gained in the process will be tapped into when considering new techniques for sensor fault accommodation.

Figure 6 – New EMA test stand at NASA Ames research center.

7. CONCLUSIONS

This paper describes efforts to identify and categorize fault modes for electro-mechanical actuators (direct-drive ball screw type in particular). Four main classes of faults are presented: mechanical/structural, motor, electrical/electronic, and sensor. A subset of faults (return channel jam, spalling, sensor bias, sensor drift, and sensor scaling) was then selected for a more detailed study and experiments on an electro-mechanical actuator test stand. The data obtained in these experiments were used for feature extraction and tests of the newly created neural-network based diagnostics system. In the process, feasibility of reliably detecting this type of faults was demonstrated. Diagnostic test results show low false positive, false negative, and misclassification rates, as well as robustness against sensor faults

ACKNOWLEDGEMENTS

The authors would like to extend their gratitude to colleagues at the Prognostic Center of Excellence, NASA Ames Research Center for their extensive assistance with this research and preparation of the manuscript. They would also like to thank Joel Rack (Moog Corporation) for his efforts in producing the experimental data, as well as Matthew Watson, Matthew Smith, and their team members at Impact Technologies for their contributions to analysis of the EMA fault modes and construction of the new actuator test facility.

REFERENCES

[1] S. C. J. Jensen, G.D. Dawson, D. , "Flight test experience with an electromechanical actuator on theF-18 Systems Research Aircraft."

[2] D. S. Bodden, Scott Clements, N. Schley *et al.*, "Seeded Failure Testing and Analysis of an Electro-Mechanical Actuator," in Aerospace Conference, 2007 IEEE, Big Sky, MT, 2007, pp. 1-8.

[3] L. U. Gokdere, S. L. Chiu, K. J. Keller *et al.*, "Lifetime control of electromechanical actuators," in Aerospace Conference, 2005 IEEE, Big Sky, MT, 2005, pp. 3523-3531.

[4] *In-Service Reliability Data of Continuously Active Ballscrew and Geared Flight Control Actuation Systems,* AIR5713, SAE Aerospace, 2006.

[5] A. Arvallo, "Condition-based Maintanence Of Actuator Systems Using A Model-Based Approach," *University of Texas, Austin*, 2000.

[6] D. T. Paul Brian Hvass, *Condition Based Maintenance For Intelligent Electromechanical Actuators*, University of Texas, Austin, 2004.

[7] M. J. Devaney, and L. Eren, "Detecting motor bearing faults," *Instrumentation & Measurement Magazine, IEEE,* vol. 7, no. 4, pp. 30- 50, 2004.

[8] K. A. Loparo, M. L. Adams, W. Lin *et al.*, "Fault detection and diagnosis of rotating machinery," *Industrial Electronics, IEEE Transactions on,* vol. 47, no. 5, pp. 1005-1014, 2000.

[9] D. Brown, G. Georgoulas, B. Zhang *et al.*, "Real-Time Fault Detection and Accommodation for Resolver Position Sensors," in IEEE International Conference on Prognostics and Health Management, Denver, CO, 2008.

[10] G. Sonnenfeld, J. Celaya, and K. Goebel, "Modeling and Analysis of Aging of IGBTs in Power Drives by Ringing Characterization," *accepted for publication in Proceedings of IEEE AUTOTESTCON*, 2008.

[11] A. Ginart, M. Roemer, P. Kalgren *et al.*, "Modeling and Analysis of Aging of IGBTs in Power Drives by Ringing Characterization," *accepted for publication in Proceedings of International Conference on Prognostics and Health Management*, 2008.

[12] K. Goebel, and W. Yan, "Correcting Sensor Drift and Intermittency Faults with Data Fusion and Automated Learning," *IEEE Systems,* vol. 2, no. 2, pp. 189-197, 2008.

[13] T. Hamada, and Y. Suyama, "EMF drift and inhomogeneity of type K thermocouples," in SICE 2004 Annual Conference, Sapporo, Japan, 2004, pp. 989- 992.

[14] S.-J. Kim, and C.-W. Lee, "Diagnosis of Sensor Faults in Active Magnetic Bearing System Equipped with Built-In Force Transducers," *IEEE Transactions on Mechatronics,* vol. 4, no. 3, pp. 180 - 186, 1999.

[15] S. Li, and P. A. Mataga, "Dynamic crack propagation in piezoelectric materials - Part II. Vacuum solution," *Journal of the Mechanics and Physics of Solids,* vol. 44, no. 11, pp. 1831-1866, 1996.

[16] D. C. Zimmerman, and T. L. Lyde, "Sensor Failure Detection and Isolation in Flexible Structires Using the Eigensystem Realization Algorithm," in 33rd Structural Dynamics and Materials Conference, Dallas, TX, 1992, pp. 2156-2166.

[17] R. O. Duda, P. E. Hart, and D. G. Stork, *Pattern Classification*, Second ed., p.^pp. 654, New York: John Wiley & Sons, Inc., 2000.

[18] M. Riedmiller, and H. Braun, "A Direct Adaptive Method for Faster Backpropagation Learning: The RPROP Algorithm," in IEEE International Conference on Neural Networks, San Fransisco, CA, 1993.

BIOGRAPHIES

Edward Balaban *is a researcher in the Diagnosis and System Health group at NASA Ames Research Center. His main areas of interest are diagnostics and prognostics of physical systems. He is currently the lead for actuator prognostics with the Diagnostics & Prognostics Group in the Intelligent Systems Division. During his years at Ames he participated in research and development of diagnostic and other autonomy elements for the X-34 experimental reusable launch vehicle, International Space Station, robotic astronaut assistants, autonomous planetary drills, and the future generation of autonomous micro-spacecraft. He received the Bachelor degree in Computer Science from The George Washington University in 1996 and the Master degree in Electrical Engineering from Cornell University in 1997.*

Abhinav Saxena *is a Staff Scientist with Research Institute for Advanced Computer Science at the Prognostics Center of Excellence, NASA Ames Research Center. His research focus lies in developing prognostic algorithms for engineering systems. He is a PhD in Electrical and Computer Engineering from Georgia Institute of Technology, Atlanta. He earned his B.Tech in 2001 from Indian Institute of Technology (IIT) Delhi, and Masters Degree in 2003 from Georgia Tech. Abhinav has been a GM manufacturing scholar and also a member of Eta Kappa Nu and Gamma Beta Phi engineering honor societies along with IEEE and ASME.*

Prasun Bansal *is an intern with Mission Critical Technologies at the Prognostics Center of Excellence, NASA Ames Research Center. His research focus lies in design & development of engineering systems and Multi Disciplinary Optimization. He earned Masters Degree in Aeronautics and Astronautics from Stanford University in 2008 and his B.Tech in Mechanical Engineering from Indian Institute of Technology (IIT) Delhi in 2006.*

Kai Goebel *received the degree of Diplom-Ingenieur from the Technische Universität München, Germany in 1990. He received the M.S. and Ph.D. from the University of California at Berkeley in 1993 and 1996, respectively. Dr. Goebel is a senior scientist at NASA Ames Research Center where he leads the Diagnostics & Prognostics groups in the Intelligent Systems division. In addition, he directs the Prognostics Center of Excellence and he is the Associate Principal Investigator for Prognostics for NASA's Integrated Vehicle Health Management Program. He worked at General Electric's Corporate Research Center in Niskayuna, NY from 1997 to 2006 as a senior research scientist. He has carried out applied research in the areas of artificial intelligence, soft computing, and information fusion. His research interest lies in advancing these techniques for real time monitoring, diagnostics, and prognostics. He holds ten patents and has published more than 100 papers in the area of systems health management.*

Paul Stoelting *received his B.S. and M.S. in Mechanical Engineering from the Rochester Institute of Technology in 1999. Paul's research focused on non-linear control theory. Currently he is pursuing a M.S. degree in Computer Science from the University at Buffalo and is researching wireless sensor-actuator networks. Paul is the Aerospace Software Engineering Manager at Moog Inc. responsible for the design, integration and deployment of embedded flight control actuation software for both Aircraft and Space vehicles. He has worked at Moog since 1996 on V-22, Comanche, Bombardier Challenger 300, X-35, F-35 and was a Staff Systems Engineer prior to moving into Software Management. He has conducted applied research on real time monitoring and prognostics for flight control actuators. His current interests are actuator network and wireless network applications for control and prognostics.*

Simon Curran *received his B.S.E.C.E. (2005) and his M.S.E.C.E. (2007) from The Ohio State University. Simon's research focused on intelligent control and humanoid locomotion. While at Ohio State he served as an assistant lecturer for The Fundamentals of Engineering for Honors program (FEH). Presently Simon works with the Aircraft System's group at Moog Inc. and spends his free time as a private pilot. His current interests are neural network applications for machine anomaly detection and network fusion*